Biotechnology and Bioprocess Engineering 26: 179-187 (2021)
DOI 10.1007/s12257-020-0143-1

pISSN 1226-8372
eISSN 1976-3816

RESEARCH PAPER

Microfluidic Single-cell Trapping and Cultivation for the Analysis of Host-viral Interactions

Reya Ganguly, Byungjin Lee, Solib Kang, Yong Sic Kim, Seong-Geun Jeong, Jae Seong Kim, So Young Park, Yamauchi Yohei, and Chang-Soo Lee

Received: 11 May 2020 / Revised: 22 September 2020 / Accepted: 22 September 2020

Abstract The isolation of single cells and their further cultivation in confined chambers are essential to the collection of statistically reliable temporal information in cell-based biological experiments. In this work, we present a hydrodynamic single-cell trapping and culturing platform that facilitates biological analysis and experimentation of virus infection into host cells. To find the optimum design of the cell trap at the microscale, we evaluated hook traps with different widths and trap intervals to obtain a high trapping efficiency of a single cell. The proposed design leverages the stochastic position of the cells as they flow into the structured microfluidic channels, where hundreds of single cells are then arrayed in nanoliter chambers for simultaneous cell-specific data collection. Optimum design is used to devise and implement a hydrodynamic cell-trapping mechanism that is minimally detrimental to the cell viability and retains a high trapping efficiency (90%), with the capability of reaching high fill factors (90%) in short loading times (10 min) in a 450-trap device. Finally, we perform an analysis of host-viral interactions under the treatment of a drug concentration gradient as a proof of concept.

Keywords: single-cell analysis, single-cell array, hydrodynamic trapping, linear drug gradient, host-viral interaction

Reya Ganguly, Byungjin Lee, Solib Kang, Yong Sic Kim, Seong-Geun Jeong, Jae Seong Kim, So Young Park, Chang-Soo Lee*
Department of Chemical Engineering and Applied Chemistry, Chungnam National University, Daejeon 34134, Korea
Tel: +82-42-821-5896
E-mail: rhadum@cnu.ac.kr

Yamauchi Yohei
School of Cellular & Molecular Medicine, University of Bristol, UK

1. Introduction

Microfluidics is a fast emerging technology that promises reductions in the cost of equipment, provides higher throughput information, and offers patient-specific therapies [1-3]. Studies have sought to establish an analytical platform for many biological events such as genetic, biochemical, and cellular analysis, with high speed, reproducibility, and throughput [4-7]. This research field is highly dynamic because of its great advantage in the operation of overall systems with very low volumes regarding cell samples as well as reagents [8]. Thus, it has become crucial to establish entire workflows for single-cell separation, isolation, and analysis.

In addition, this approach enhances the ability to precisely monitor signaling dynamics at the single-cell level such as viral infections of a host cell or cancer metastasis [9,10]. For example, the most widely used approach, the plaque assay, is able to analyze virus infection. The total number of plaques formed or inhibited by drug treatment is counted for the screening of viral drugs [11]. Although the plaque assay provides sufficient information and flexibility in conventional biological lab protocols, it is hard to obtain precise quantitative information required for complete eradication of infectious viral particles.

Another important issue in the microfluidic approach is the analysis of a large number of single cells in a high-throughput manner. For example, conventional microwell platforms allow random capturing of thousands of single cells by the gravitational pull to enable cell culture-based analysis [12-15]. However, these devices limit the dynamic flow of culture media as well as active manipulation of the trapped cells such as exposure to stimuli or drugs. To overcome this weakness, an integration of microfluidic valves, optical tweezers, dielectrophoresis (DEP), and

acoustic waves within a microfluidic device has been proposed for real-time monitoring and manipulation of a single cell [3,16,17]. However, these methods have difficulties such as cytotoxic low-conductivity buffers, high temperatures induced by Joule-heating, accidental cell lysis resulting from high current usage, complexity in microfabrication, and efficiency of single-cell trapping [18-20].

In this study, we optimize the design of the cell trap microstructure in a microfluidic device to improve the efficiency in single-cell trapping in a high-throughput manner. The integration of real-time monitoring and manipulation of a single-cell with the formation of a concentration gradient of an antiviral drug is useful for analyzing host cell-viral interactions in the presence of different concentrations of drug applied. Moreover, we remove the side effects of fluid shear stresses over the cells, which leads to impaired cell survival and relatively uncertain position accuracy during long-duration experiments.

2. Material and Methods

All chemicals employed in this study were of analytical or research grade. The chemicals used in this study for fabrication techniques are SU-8 3025 (Microchem, USA) and poly-(dimethyl siloxane) (PDMS) (Dow Corning sylgard 184, Seoul, Korea). Media for cell culture include Dulbecco's modified Eagle medium (DMEM), fetal bovine serum (FBS), penicillin-streptomycin, and OptiPrep solution (Capricorn scientific GmbH, Germany). Other materials for Host-viral interaction studies include bafilomycin A1, Leibovitz's L-15 medium, 4-(2-hydroxyethyl)-1-piperazineethanesulfonic acid (HEPEs), bovine serum albumin (BSA), and influenza A virus (Capricorn scientific GmbH, Germany), as well as cell line ACHN (ATCC CRL-1611), A549 (ATCC CCL-185), and HEPG2 (ATCC HB-8065). The total fluorescent intensity recorded across the detection channel on an inverted florescent microscope (TE2000, Nikon, Japan) equipped with a CCD camera (Coolsnap cf, photometrics, USA). The images were captured and analyzed by an Image-pro plus software (Media Cybernetics, Newburyport, MA).

2.1. Design and fabrication of cell trapping device

Using Auto-CAD software, we designed our device and obtained a negative photomask of the design. The wafer mold was then prepared, followed by the fabrication of a PDMS single-layer microfluidic device by soft lithography. In these cases, we used SU-8 3025 negative photoresist to fabricate 25 μm thick channels. The SU-8 3025 photoresist was partially spread for 10 s at 500 rpm over a 4-inch silicon wafer followed by complete spreading at 3100 rpm for 30 s. After baking the coated wafer at 95°C for 10 min 8 s, the wafer was cooled to room temperature and subsequently exposed to UV (16 mJ/16 mW) light for 25 s. The wafer was post-baked at 95°C for 3 min 33 s and finally developed with a SU-8 developer for 5 min. After salinization of the wafer, the PDMS mixture (10:1 ratio) was poured onto the wafer mold and heated for 30 min at 65°C, a process called curing. The PDMS was peeled off, cut to the appropriate size and punched. The device was attached to a glass after plasma treatment for 1 min.

To achieve single-cell trapping, we fabricated a microfluidic device with various dimensions to acquire sufficient statistically significant data to reach an acceptable conclusion. As the experiments were mainly focused on the efficacy to trap cells, we thus selected hook type trap structures for further study. However, the device has two upper inlets (media, virus, and drug), one common cell inlet and outlet at the bottom of the device and 9 individual outlets. A total of 9 channels per chip is accommodated with 50 trap structures facing the upper inlet channel and placed alternately to each other along both walls of the channel (Fig. 1). The variable dimensions are the width between two trap structures in the opposite wall where the trap structure was placed in an alternate manner and trap interval, the gap between two traps along the same wall. The final design of the device to study host-viral interactions was optimized in terms of the channel width (75 and 100 μm) and trap interval (60, 80, 100, and 120 μm) to achieve a linear drug gradient and high efficiency in cell trapping.

2.2. Cell culturing

The cell line A459 (ATCC) was cultured in DMEM supplemented with 10% (vol/vol) FBS and 1% penicillin-streptomycin, and the solution was then filtered with a 0.2 μm filter (this solution is hereafter referred to as complete DMEM). The cells were then incubated at 37°C in a humidified atmosphere with 5% CO_2. Before experimenting, the viability and count of cells were always checked using a hemocytometer and trypan blue (an azo dye) staining. Based on the cell counting data, the desired concentration of cells was prepared in 16% OptiPrep complete DMEM media.

2.3. Microfluidic device operation for cell trapping

The device was primed before cell loading with complete DMEM media from the inlet using a syringe pump. Injection of cells was carried out for 20 min with a flow rate of 90 μm/h to achieve a final flow rate of 5 μm/h in each channel at 24°C and 16% humidity. The excess untrapped cells were then removed by allowing the 3rd round of flow of complete DMEM media until the channels were clear. The trapped cells were then imaged and counted

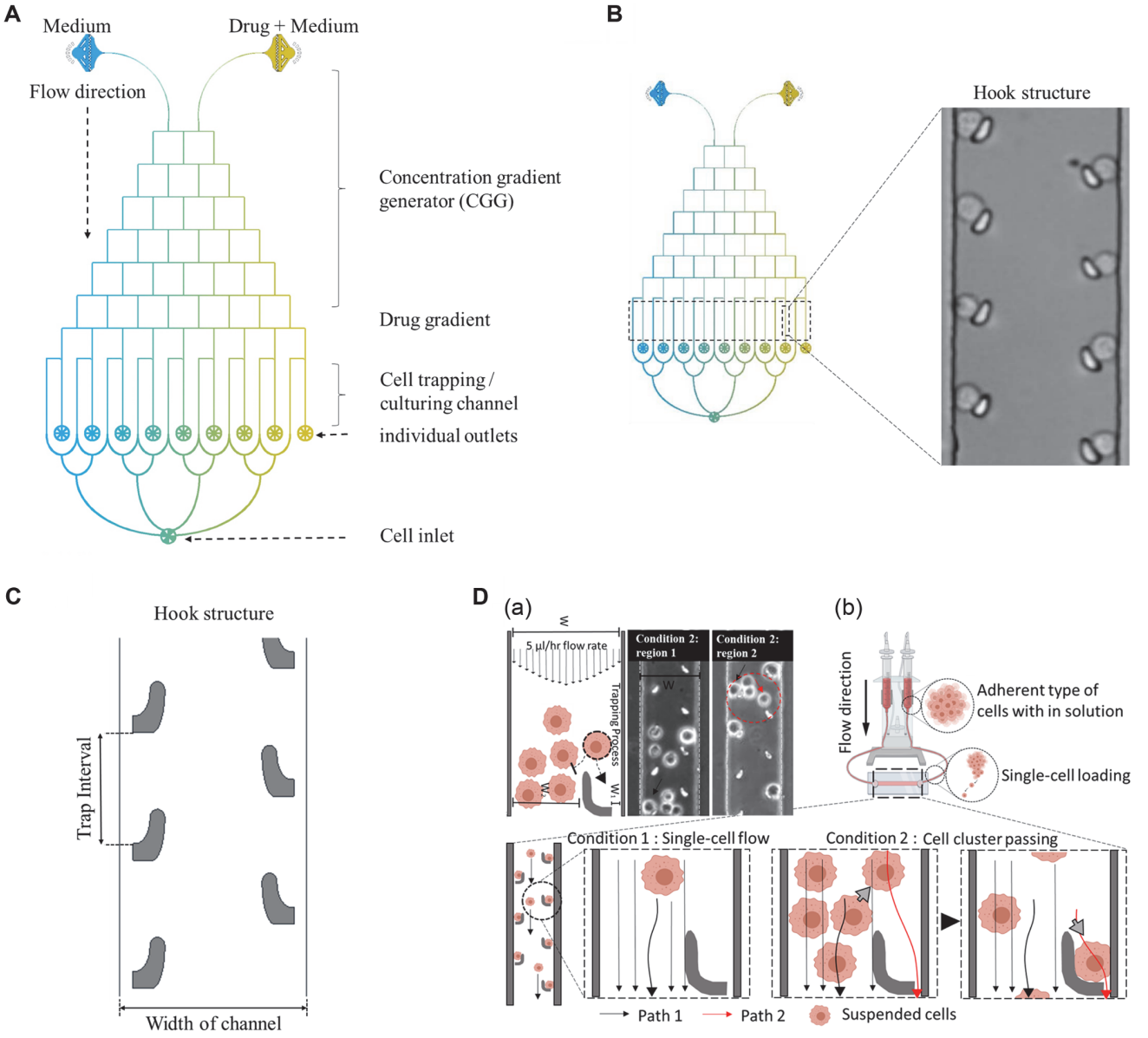

Fig. 1. Basic design of the microfluidic device generating a concentration gradient of chemical drugs coupled with a trap array for single-cell trapping and in situ analysis. (A) Device structure consists of two input lines for two solutions (medium and drug containing medium), a common cell inlet, gradient generating part and individual outlets. (B) Magnified optical image showing the hook trap structure after cell trapping. (C) Schematic diagram indicating the trap interval and trap width along the microchannel. (D) Schematics of fluid dynamics for trapping cells in hook design. (a) The figure shows the flow direction of fluid based on Zweifach-Fung bifurcation law at channel bifurcation, which is comparable to bifurcation near hook trap vicinity. This causes large number of cell pass through W2, during this time some cells are pushed to be trapped as W2 is temporarily blocked by cells. (W: width). An optical image of two different regions within the channel is shown to support the hypothesis (black arrow). (b) Show two possible condition, condition 1 when single cell flow it passes from W2 (Path 1) and do not get trapped whereas when cluster of cells as in condition 2, one cell close to trap structure is pushed towards W1 and get trapped (Path 2).

to check the trap structure efficiency. The same procedure was followed during the host-viral interaction study where after cell trapping, the device was further injected with virus-containing media and drug-containing media. A detailed explanation is given in the following sections.

2.4. Drug concentration preparation and estimation of gradient formation by fluorescent dye

To prepare the drug gradient, 1 µL of 100 nM bafilomycin A1 was dissolved in 1 µL of dimethyl sulfoxide (DMSO) and 998 µL of infection media. This solution was infused

through any one of the two inlets, using the other inlet only for infusing infection media.

The simple principle of laminar flow and diffusion within the microfluidic channel allows the mixing of two solutions down the Christmas tree. The estimation of the most suitable flow rate and concentration to achieve a linear gradient was performed with fluorescein sodium salt. It is also possible to determine the concentration at the observation site. The concentration of fluorescent molecule (c) at the observation area is given by C = 1/1+k where k is the ratio of the flow rate of the buffer (V_b) and fluorescent molecule (V_f), given by $k = V_b/V_f$. C = 1/1+k is valid only if K = 0, α, or $0.1 \leq k \leq 9$ [21].

2.5. Virus infection and bafilomycinA1 gradient generation in a microfluidic device

To allow effective infection by the influenza A virus, we used Leibovitz's L-15 medium with 50 mM HEPEs and 0.2% BSA. Hereafter we refer to this medium as the infection medium throughout the paper. Influenza A virus labeled with DiOC18 (green) and R18 (red) was dissolved in warm infection medium to saturation. To allow infection of the trapped cells, virus was dissolved in two different media. The first medium contained both drug and virus (Total virus concentration in the final solution before infusion being 2 × 106 PFU/mL), and the composition included 100 μL of virus, 0.3 μL of bafilomycin A1, 0.3 μL of DMSO, and 199.4 μL of infection media. The second medium contained 100 μL of virus dissolved in 0.6 μL of DMSO and 199.4 μL of infection media. Injecting media from inlet 1 and inlet 2 caused the formation of a drug gradient and uniform distribution of virus within the channel. We incubated the device for 3 h at 37°C, followed by washing of excess virus with phosphate-buffered saline (PBS) and fixing cells with 4% formaldehyde for imaging.

3. Results and Discussion

3.1. Device design and single-cell capture efficiency

The microfluidic architecture was designed to integrate gradient generating microchannels with an array of hydrodynamic traps to capture and culture single-cells for the analysis of single-cell-virus interactions at various drug concentrations (Fig. 1A). Firstly, the basic design of trapping microfluidic device follows the principle of Zweifach-Fung bifurcation law [22]. The formula is given by:

$$\frac{R_2}{R_1} = \left(\frac{L2}{L1}\right) \cdot \left(\frac{a2+b2}{a1+b1}\right)^2 \cdot \left(\frac{a1}{b2}\right)^3 \cdot \left(\frac{1+\frac{5a1}{6b1}}{1+\frac{5b2}{6a2}}\right)$$

Where R is resistance to flow, L is the path length, a is path depth, b is path width, 1 and 2 indicating related to path 1 and path 2 respectively [23]. Path 1 and 2 have different resistance that depends on channel width as shown in the formula. Secondly, at low cell density almost all cell passes through the wide (W_2) side in the channel, however at high cell density the wide side is temporarily blocked by cluster of cells which forces an individual cell to pass through the narrow side and get trapped [22]. The continuous fluid flow will immediately clear such temporary blocks. This crowding and trapping process takes place throughout the entire channel, hence we chose to optimize trap interval to allow single cluster to cause trapping in multiple traps. (Fig. 1D, a). To achieve the high efficiency of single-cell trapping and a linear drug gradient, we simultaneously optimized several key parameters. To achieve the linear drug gradient, two parameters were considered, which are, concentration of fluorescein sodium salt (10 μM, 100 μM, and 1,000 μM) (Fig. S1A) and flow rate of infusing sample (1 μL/h, 5 μL/h, and 10 μL/h) (Fig. S1B). To design most efficient cell trapping design various channel widths (75 μm and 100 μm) and trap intervals (60 μm, 80 μm, 100 μm, and 120 μm) were investigated for trap arrays to enable more cells to be analyzed at one time. The height of the channel was maintained at 25 μm. The device that worked best has traps that are arranged in independently accessible lanes; 9 trapping channels are connected to each other parallel. Each chamber consisted of 50 cell traps with alternating arrangements (Fig. 1). These hydrodynamic traps utilized differences in hydrodynamic resistance [23,24] between the trapping pocket and a bypassing fluidic stream to deterministically capture single cells (Fig. 1D).

After infusing cells into the device for 20 min, the efficiency of single-cell trapping was calculated as the ratio of the total number of single cells trapped to the total number of trap structures within each channel. When performing cell trapping at the micron scale, the fluid in the channel is known to exert viscosity and shear stress over cells moving along the channel. These effects are directly reflected by the cell trapping efficiency of the device; thus, we have to find the optimum flow rate for high efficiency. Preliminarily, our experiment showed that 5 μL/h infusion was appropriate at a cell density of 2×10^6 cells/mL. We observed that 1 μL/h per channel showed no cell trapping whereas 10 μL/h per channel expanded the chip and deformed the cell. Additionally, we investigated the effect of the cell density over the optimized dimensions of the microfluidic device and flow rate on cell trapping efficiency but did not observe any significant difference.

The cell trapping efficiency did not differ significantly among hook structures with different dimensions (Fig. 2); since the trapping depends on the chances when a cluster

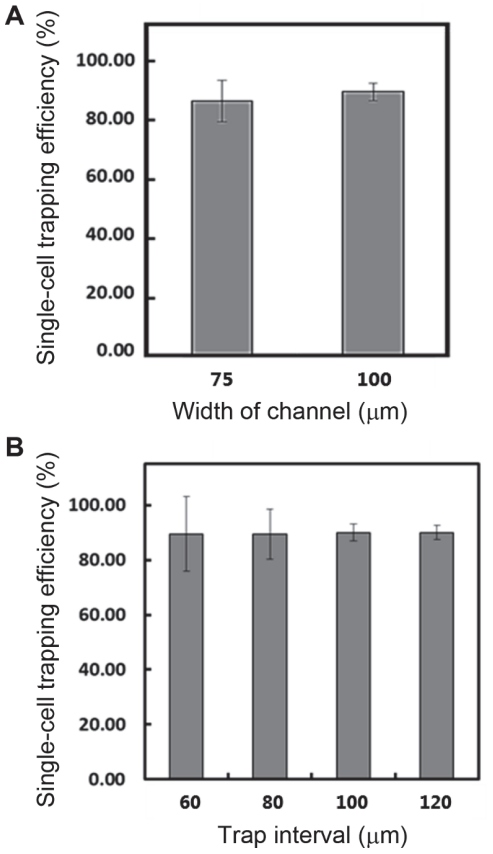

Fig. 2. Single-cell trapping efficiency of hook type structures. (A) different channel widths at constant trap intervals of 60 μm and (B) different trap intervals at constant widths of 100 μm.

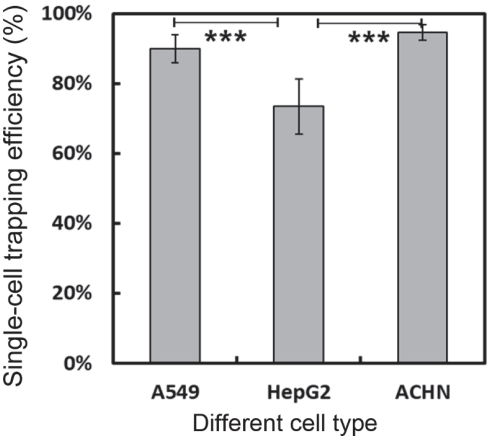

Fig. 3. Effect of different cell types (A549, HepG2, and ACHN) on the cell trapping efficiency with the hook structure (60 μm trap interval and 100 μm channel width). Statistical significance: ***$P < 0.0001$ by Student's *t*?test.

of cell near the vicinity of a trap will arise so that a cell will be trapped in the nearest hook trap while other cells reaches to the next trap. Hence, it can be expected that if the trap interval is placed close to each other, a single cluster can cause cell trapping simultaneously in many traps before the temporary blockage is cleared (Fig. 1D, a). Thus, even though the different trap interval did not show significant differences, we chose the minimum trap interval to get maximum advantage of the above hypothesis. Additionally, placing traps at a minimum distance help to accommodate many traps at a single channel. Thus, in spite of no significant difference between dimensions we selected a 60 μm trap interval and 100 μm width. The 100 μm width was selected to additionally ensure avoiding the possibility and frequency of permanent channel blocking instead of temporary blockage by clusters of cells during cell infusion. Based on the optimized microfluidic device, we can rapidly and continuously introduce medium through the channels while maintaining minimal flow across the traps to ensure constant nutrient repletion with low and uniform shear stress on the cells. The cells in the device was exposed to gentle flow rate, PDMS trap design with no sharp edges favored by gas permeability feature of PDMS. Hence, this design was suitable to retain cell viability for 8 h (Fig. S2A). In addition we show the viability of cells before and after loading to the device to be 84.35% and 70.714% respectively with p value equal to 0.0288 (Fig. S2B and C). Independent flow control also allows for rapid buffer exchange without dislodging trapped cells, thus enabling the on-chip implementation of biological cell analysis, for example, host-viral interactions in this study. In addition, we investigated several adhesive cell lines such as ACHN (ATCC CRL-1611), A549 (ATCC CCL-185), and HEPG2 (ATCC HB-8065) in order to evaluate the trapping efficiency across different cell diameters. Equivalent to other reported devices [25-28], this approach leads to an efficient capture rate. However, the trapping efficiency largely depends on the size of the cell and the gap between the trap structure and the channel wall. Cells are flexible and can be squeezed easily [22], thus, because of this property the cells in the size range of 8 μm to 12 μm or above can be trapped effectively. Cells with size below this range will easily escape (Fig. S3). Thus, the gap needs to be optimized based on the size of the cell to yield better trapping statistics. We further checked the effect of the flow rate on the trapping efficiency of these cells. Our observation shows 94%-97% trapping efficiency in different cell types (Fig. 3).

3.2. Diffusion-based gradient generator

The gradient formation in the microchip with two inlets was investigated to precisely control the various concentrations generated. To quantify the concentration gradient, fluorescein isothiocyanate (10 μM, 100 μM, and 1000 μM FITC) and buffer solution were introduced from the left and right inlets. To evaluate the intensity of the fluorescent solution at the output, a grayscale image algorithm was

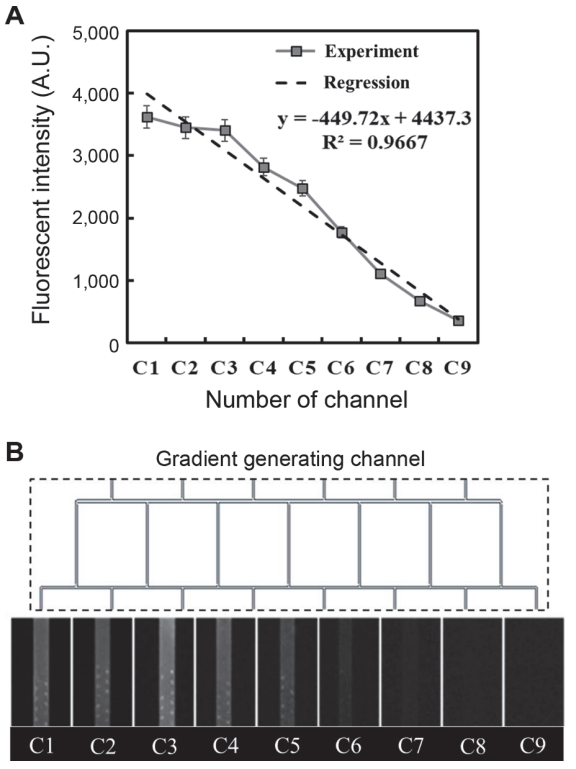

Fig. 4. Formation of a linear concentration gradient. (A) A plot of fluorescent intensity at each channel under optimum conditions (hook trap with a 60 μm trap interval and 100 μm channel width, 100 μM fluorescein sodium salt at a flow rate of 5 μL/h). (B) The fluorescence image shows the linear concentration gradient of FITC.

taken, in which each image indicates the light intensity matrix of image pixels. The plot showing the intensity profile across the outlet channel was taken while maintaining a steady flow through the microfluidic network (same fluid flow rate at both inlets) (Fig. 4). We investigated linear-gradient generation under different flow rates: 1 μL/h, 5 μL/h, and 10 μL/h. This device was then optimized to obtain a linear gradient, *i.e.*, the concentration output of the device with a predictable distribution. The parameter considered for gradient generation was the fluid flow rate, which was fixed to 1 μL/h, 5 μL/h, and 10 μL/h as well as different concentrations of the FITC solution (10 μM, 100 μM, and 1000 μM) (Fig. 4).

The optimum dimension was fixed at a 100 μm channel width and 60 μm trap interval of the hook type trap structure. Here, we utilized our optimized device for further analysis and proof of concept. The concentration profile at the outlet can be predicted by understanding the splitting ratio of flow at the branching point of the network. The principle behind gradient generation using a Christmas tree design is based on controlled diffusive mixing of fluids under laminar flow. The diffusion coefficient characterizes the diffusion of solute species in diluent species based on Fick's first law of diffusion [29]. Fick's second law explains that mass transport via diffusion is an un-steady process and changes with time [29]. Hence, these two laws convey the concept of the diffusion process in a microfluidic domain. Fig. 4 shows that 100 μM FITC flowing at 5 μL/h showed the highest linearity. This condition provides the optimum time required for the diffusive mixing of the laminar streams flowing in the microchannels. Thus, we selected a concentration of 100 μM and a flow rate of 5 μL/h as the optimum parameters to generate a linear gradient of the drug (Fig. 4). In addition, a convection-based gradient generator, which depends on the fluid flow field, induces shear stress to downstream trapped cells. The channel wall experiences maximum shear stress, τ_{max}, which can be determined by the parallel-plate flow approximation [30].

$$\tau_{max} = 6\mu Q/wh^2 \quad (1)$$

where τ_{wall} is the shear stress induced by the flow rate (Q), in microchannels of height (h), width (w), and the dynamic viscosity of the fluid flowing is given by μ. This equation (Eq. 1) thus defines the linear proportional relationship between the shear stress and flow rate. Hence, at a low flow rate, upon completion of diffusive mixing, a homogeneous solution of intermediate concentration is obtained, which when fed into downstream channels with trapped cells is expected to render lower shear stress.

3.3. Host-viral interaction study

Single-cell heterogeneity provides an unprecedented resolution of host cell behavior upon infection. Single-cell infection with the virus is reported to show host heterogeneity at the cell type and cell state levels [31,32]. In addition, viral heterogeneity at the genome sequence level occurs due to polymorphisms of active viral particles or mutations in transcripts. Influenza A is an extensively studied virus, as it is known for its major impact on human health [33]. Moreover, the dynamics of infection and associated cell types are poorly explored. These challenges are partly because animal models do not perfectly recapitulate the human system.

To test our device, we performed a host-viral interaction study as a proof of concept using the influenza A virus [34]. Fig. 5 illustrates the quenching of fluorescence when DiOC18 and R18 are close together. The fluorescence of DiOC18 is quenched by R18; however, R18 also shows partial self-quenching. The fusion of the membrane increases the distance between these molecules, exceeding the critical distance for quenching gives green fluorescence, which is dominant over red. This result indicates a successful infection. As expected, the gradient channel shows a linear gradient of bafilomycin A1. Under this

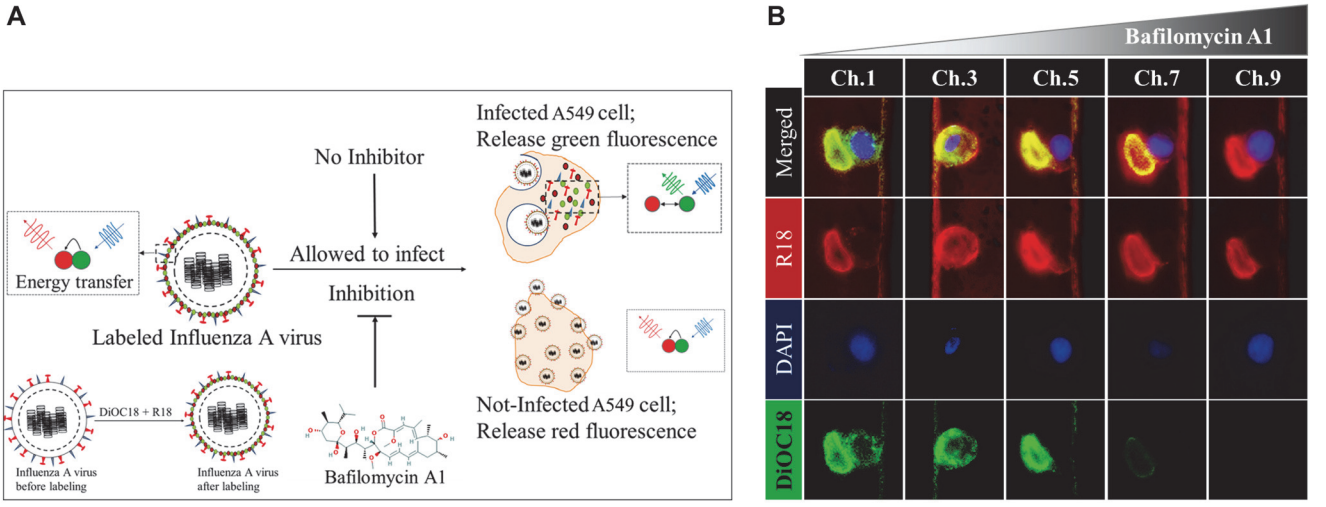

Fig. 5. Investigation of host-viral interactions under a concentration gradient of bafilomycin A1. (A) Schematic representation of infection by labeled virus in the presence or absence of bafilomycin A1 and the principle behind the representative fluorescence. (B) The fluorescence images show real-time host-viral interactions at different concentrations of bafilomycin A.

concentration gradient, when trapped single cells were exposed to virus particles, a similar gradient effect was observed in terms of the infection phenomena. It is observable that channel 9, which has maximum bafilomycin A1 do not emit green fluorescence but does present red fluorescence; thus, even though the viruses are present in the trap site, it failed to infect cells at the highest concentration of bafilomycin A1. The gradual increasing effect of green fluorescence from channel 9 to channel 1 depicts successful host-viral interaction monitoring under different concentrations of drug stress using our device. This result also indicates that viruses retain their integrity and fusogenicity in this device. Hence, this platform can efficiently trap single cells and enable cell monitoring of interactions with other biological factors. Viral fusion is a quick process associated with rapid pH change. In a conventional dequenching assay, the involvement of a large volume might result in asynchronous triggering, leading to uncertain timing of the pH drop. This effect will obscure the pH dependence of fusion viruses. Therefore, the overall reduced volume in this on-chip assay will facilitate rapid mixing within a short period, thus partially reproducing the infection microenvironment.

4. Conclusion

Investigating viral infection at the single-cell level using a microfluidic platform provides a more precise understanding of the interactions. This approach provides advantages for live imaging and observation of host-viral interactions for screening inhibitory compounds. Here, we have successfully determined the concentration gradient of a candidate drug while maintaining accurate physical factors such as temperature and pH, which might alter the infection outcome. To achieve this aim, we first optimized our single-cell trap structure to make a single-cell array within a short time and minimize cell loss, in addition to avoiding cell clogging, which is a very common problem when using adherent mammalian cells. The trapping efficiency of the device reached 90% on average. The optimized device dimensions were a 100 μm channel width and a 60 μm trap interval. In addition, a flow rate of 5 μL/h and a concentration of 100 μM were standardized to generate a linear drug gradient. After optimizing the conditions, we investigated the trapping efficiency for different types of cells, which was approximately 94%-97%. Additionally, we checked the performance of our device for host-viral interaction studies. We showed the effect of the drug gradient on the infection. In conventional studies, physical factors, population bias, and experimental microenvironment are difficult to maintain precisely. Our microfluidic-based platform provides a more controlled and biologically relevant model system for studying viral infection biology. Viral infections are significantly affected by the physical and chemical properties of the microenvironment; thus, we believe that our approach has provided a stable and controlled experimental condition for clear investigation.

In summary, few studies consider microfluidics as another platform for answering several important questions in the field of virology, although there is continuous growth in studies of viral infection biology using conventional methods. Through our research, we have established a platform to analyze the effect of inhibitory molecules

against viruses when they are in close contact with their preferred host. We monitored the host-viral interaction during treatment with bafilomycin A1, which is known to inhibit viral-endosome membrane fusion. In our microfluidic approach, a wide range of host-viral analyses can be performed under different concentrations of drugs. Thus, we not only focus on the interaction behavior against drugs but also simultaneously predict the precise minimum concentration of the drug required for complete inhibition. Future research needs to focus more on newly evolving viruses. Many fields of research, however, are helping science to efficiently detect viruses, such as conventional PCR and multiplex PCR, nanomaterials, LFTs [35-39], but recent outbreaks of emerging viruses are causing mass destruction. These emerging viruses are considered to cross the barriers of genetic variation and move from one species to another. Even though many macroscale studies are being performed worldwide, they do not provide an unbiased population analysis. Thus, understanding of viral behavior must be given top priority. To date, a precise understanding of the factors influencing viruses to re-establish their host remains unclear. Hence, we envision microfluidics as a strong candidate along with other multidisciplinary approaches to better understand principles that influence viruses to jump species barriers.

Acknowledgements

This research was supported by Chungnam National University research fund.
The authors declare no conflict of interest.
Neither ethical approval nor informed consent was required for this study.

Electronic Supplementary Material (ESM)

The online version of this article (doi: 10.1007/s12257-020-0143-1) contains supplementary material, which is available to authorized users.

References

1. Martin, R. M., H. Leonhardt, and M. C. Cardoso (2005) DNA labeling in living cells. *Cytometry A.* 67: 45-52.
2. Wlodkowic, D., J. Skommer, and Z. Darzynkiewicz (2008) SYTO probes in the cytometry of tumor cell death. *Cytometry A.* 73: 496-507.
3. Andersson, H. and A. van den Berg (2004) Microtechnologies and nanotechnologies for single-cell analysis. *Curr. Opin. Biotechnol*. 15: 44-49.
4. Beebe, D. J., G. A. Mensing, and G. M. Walker (2002) Physics and applications of microfluidics in biology. *Annu. Rev. Biomed. Eng.* 4: 261-286.
5. El-Ali, J., P. K. Sorger, and K. F. Jensen (2006) Cells on chips. *Nature.* 442: 403-411.
6. Hong, J. W. and S. R. Quake (2003) Integrated nanoliter systems. *Nat. Biotechnol.* 21: 1179-1183.
7. Walker, G. M. and D. J. Beebe (2002) A passive pumping method for microfluidic devices. *Lab. Chip.* 2: 131-134.
8. Hosseini, F. and M. Rahimi (2020) Experimental study and artificial intelligence modeling of liquid-liquid mass transfer in multiple-ring microchannels. *Korean J. Chem. Eng.* 37: 411-422.
9. Di Carlo, D., L. Y. Wu, and L. P. Lee (2006) Dynamic single cell culture array. *Lab. Chip.* 6: 1445-1449.
10. Lindstrom, S. and H. Andersson-Svahn (2010) Overview of single-cell analyses: microdevices and applications. *Lab. Chip.* 10: 3363-3372.
11. Harmon, M. W. (1982) Diagnostic virology: illustrated by light and electron microscopy. G. D. Hsiung. *Q Rev. Biol.* 58: 600.
12. Dusseiller, M. R., D. Schlaepfer, M. Koch, R. Kroschewski, and M. Textor (2005) An inverted microcontact printing method on topographically structured polystyrene chips for arrayed micro-3-D culturing of single cells. *Biomaterials*. 26: 5917-5925.
13. Khademhosseini, A., J. Yeh, S. Jon, G. Eng, K. Y. Suh, J. A. Burdick, and R. Langer (2004) Molded polyethylene glycol microstructures for capturing cells within microfluidic channels. *Lab. Chip*. 4: 425-430.
14. Kobel, S., M. Limacher, S. Gobaa, T. Laroche, and M. P. Lutolf (2009) Micropatterning of hydrogels by soft embossing. *Langmuir*. 25: 8774-8779.
15. Ogunniyi, A. O., C. M. Story, E. Papa, E. Guillen, and J. C. Love (2009) Screening individual hybridomas by microengraving to discover monoclonal antibodies. *Nat. Protoc*. 4: 767-782.
16. Johann, R. M. (2006) Cell trapping in microfluidic chips. *Anal. Bioanal. Chem.* 385: 408-412.
17. Voldman, J. (2006) Electrical forces for microscale cell manipulation. *Annu. Rev. Biomed. Eng.* 8: 425-454.
18. Huang, W. H., W. Cheng, Z. Zhang, D. W. Pang, Z. L. Wang, J. K. Cheng, and D. F. Cui (2004) Transport, location, and quantal release monitoring of single cells on a microfluidic device. *Anal. Chem.* 76: 483-488.
19. Mittal, N., A. Rosenthal, and J. Voldman (2007) nDEP microwells for single-cell patterning in physiological media. *Lab. Chip.* 7: 1146-1153.
20. Seger-Sauli, U., M. Panayiotou, S. Schnydrig, M. Jordan, and P. Renaud (2005) Temperature measurements in microfluidic systems: heat dissipation of negative dielectrophoresis barriers. *Electrophoresis*. 26: 2239-2246.
21. Park, J. W., H. S. Shin, H. J. Kim, and N. L. Jeon (2014) Concentration gradient generation and control. In: D. Li (ed.). *Encyclopedia of Microfluidics and Nanofluidics*. Springer, Boston, MA, USA.
22. Zhang, K., C. K. Chou, X. Xia, M. C. Hung, and L. Qin (2014) Block-Cell-Printing for live single-cell printing. *Proc. Natl. Acad. Sci. U S A.* 111: 2948-2953.
23. Shi, W. W., J. Qin, N. Ye, and B. Lin (2008) Droplet-based microfluidic system for individual *Caenorhabditis elegans* assay. *Lab. Chip.* 8: 1432-1435.
24. Skelley, A. M., O. Kirak, H. Suh, R. Jaenisch, and J. Voldman (2009) Microfluidic control of cell pairing and fusion. *Nat. Methods.* 6: 147-152.
25. Chen, P., S. Yan, J. Wang, Y. Guo, Y. Dong, X. Feng, X. Zeng, Y. Li, W. Du, and B. F. Liu (2019) Dynamic microfluidic cytometry for single-cell cellomics: High-throughput probing single-cell-resolution signaling. *Anal. Chem.* 91: 1619-1626.

26. Ohiri, K. A., S. T. Kelly, J. D. Motschman, K. H. Lin, K. C. Wood, and B. B. Yellen (2018) An acoustofluidic trap and transfer approach for organizing a high density single cell array. *Lab. Chip.* 18: 2124-2133.
27. Carlo, D. D. and L. P. Lee (2006) Dynamic single-cell analysis for quantitative biology. *Anal. Chem.* 78: 7918-7925.
28. Wang, Y., X. Tang, X. Feng, C. Liu, P. Chen, D. Chen, and B. F. Liu (2015) A microfluidic digital single-cell assay for the evaluation of anticancer drugs. *Anal. Bioanal. Chem.* 407: 1139-1148.
29. Ahmed, T., T. S. Shimizu, and R. Stocker (2010) Bacterial chemotaxis in linear and nonlinear steady microfluidic gradients. *Nano. Lett.* 10: 3379-3385.
30. Deen, W. M. (1998) *Analysis of Transport Phenomena.* 1st ed., p. 433. Oxford University Press, New York, NY, USA.
31. Steuerman, Y., M. Cohen, N. Peshes-Yaloz, L. Valadarsky, O. Cohn, E. David, A. Frishberg, L. Mayo, E. Bacharach, I. Amit, and I. Gat-Viks (2018) Dissection of influenza infection *in vivo* by single-cell RNA sequencing. *Cell Syst.* 6: 679-691.e4.
32. Russell, A. B., C. Trapnell, and J. D. Bloom (2018) Extreme heterogeneity of influenza virus infection in single cells. *Elife.* 7: e32303.
33. Yang, J. M., K. R. Kim, and C. S. Kim (2018) Biosensor for rapid and sensitive detection of influenza virus. *Biotechnol. Bioprocess Eng.* 23: 371-382.
34. Hong, G. P., J. H. Park, H. H. Lee, K. O. Jang, D. K. Chung, W. Kim, and I. S. Chung (2015) Production of influenza virus-like particles from stably transfected *Trichoplusia ni* BT1 TN-5B1-4 cells. *Biotechnol. Bioprocess Eng.* 20: 506-514.
35. Hwang, C. H., S. G. Jeong, H. K. Park, C. S. Lee, and Y. G. Kim (2016) Paper-based neuraminidase assay sensor for detection of influenza viruses. *Korean Chem. Eng. Res*. 54 : 380-386.
36. Hwang, B. H., H. H. Shin, and H. J. Cha (2017) Optimization of DNA microarray biosensors enables rapid and sensitive detection. *Biotechnol. Bioprocess Eng.* 22: 469-473.
37. Hong, W., S. G. Jeong, G. Shim, D. Y. Kim, S. P. Pack, and C. S. Lee (2018) Improvement in the reproducibility of a paper-based analytical device (PAD) using stable covalent binding between proteins and cellulose paper. *Biotechnol. Bioprocess Eng.* 23: 686-692.
38. Bae, J. E. and I. S. Kim (2010) Multiplex PCR for rapid detection of minute virus of mice, bovine parvovirus, and bovine herpesvirus during the manufacture of cell culture-derived biopharmaceuticals. *Biotechnol. Bioprocess Eng.* 15: 1031-1037.
39. Lee, C. S., S. H. Lee, Y. G. Kim, M. K. Oh, T. S. Hwang, Y. W. Rhee, H. M. Song, B. Y. Kim, Y. K. Kim, and B. G. Kim (2006) Fabrication of disposable protein chip for simultaneous sample detection. *Biotechnol. Bioprocess Eng.* 11: 455.